Melting-Curve Extrema from a Repulsive "Step" Potential*

D. A. Young and B. J. Alder
Lawrence Livermore Laboratory, University of California, Livermore, California 94550
(Received 14 March 1977)

Molecular dynamics calculations in two dimensions for particles interacting with a repulsive "step" potential show melting-curve maxima and minima as well as solid-solid phase transitions. These features are similar to those observed in the phase diagram of cesium and cerium.

The melting temperatures[1] of most elements and simple compounds increase monotonically with pressure. Those few phase diagrams which show maxima and minima in the melting temperature are usually ascribed to the coexistence of loosely packed solid phases with more dense liquids, as in the case of water. Two of the most interesting phase diagrams, however, are those of the elements cesium and cerium, in which *close-packed* solid phases are in equilibrium with more dense liquids. The cerium phase diagram[2] [Fig. 1(a)], with a melting-temperature minimum, shows in addition an fcc-fcc isostructural phase transition which ends in a critical point. The cesium phase diagram[3] [Fig. 1(b)], with two closely spaced melting-temperature maxima, shows a similar fcc-fcc phase transition which, however, terminates in a triple point on the melting curve. Analysis of shock-wave experiments on rare-earth elements suggests that similar melting-curve extrema are not uncommon among the elements.[4]

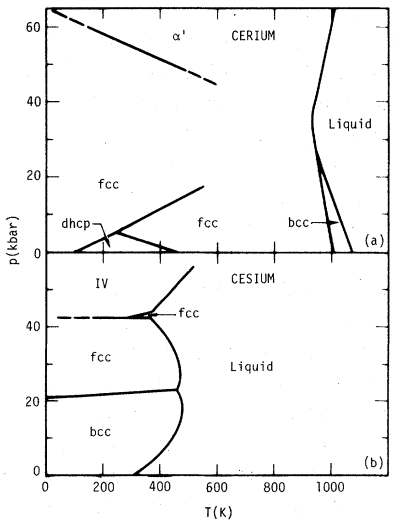

FIG. 1. The phase diagrams of cerium (a) and cesium (b). The high-pressure phases Ce α' and Cs IV are not well characterized.

The solid-solid isostructural transitions strongly suggest that upon compression the valence electrons shift into vacant orbitals.[5] In cesium the transition has been ascribed to a $6s \rightarrow 5d$ electron promotion, and in cerium to a $4f \rightarrow 5d$ promotion. In both cases the effective atomic size in the solid undergoes an abrupt decrease at the transition. In the liquid, however, the configurational disorder allows the electronic shift to occur over a broad pressure range, with the result that the liquid is more dense than the solid until the solid transition pressure is reached.[2,3]

A number of statistical-mechanical models[6] have been proposed which exhibit some of the properties of the Ce and Cs phase diagrams, and which invoke interparticle potentials which allow the particles to "collapse" under compression. These models all make important approximations, such as the use of cell models or perturbation theory, and it is not clear to what extent the conclusions are thereby invalidated.

In this Letter we describe molecular dynamics calculations in which no assumption, other than the form of the interparticle potential, is made. Thus a rigorous relationship between the potential and the resulting phase diagram is obtained.

The potential $\varphi(r)$ between two particles separated by a distance r is chosen to be a repulsive "step" or an inverted square well with a hard core:

$$\varphi(r) = \infty, \quad 0 \leq r < \sigma,$$

$$\varphi(r) = \epsilon, \quad \sigma \leq r < c\sigma,$$

$$\varphi(r) = 0, \quad c\sigma \leq r.$$

At low temperatures ($kT \ll \epsilon$) and pressures the particles all have an effective diameter $c\sigma$, while at high pressures and temperatures the particles have an effective diameter σ. At intermediate pressures and temperatures the transition between these limits can be expected to lead to phase transitions similar to those shown in Fig. 1.

The molecular dynamics calculations have been carried out in two dimensions in order to see clearly the various solid-liquid phase boundaries, since the solid metastability found in three-dimensional hard-sphere systems[7] makes the melting point difficult to locate. We expect no qualitative difference between the phase diagrams in two and three dimensions. In these calculations, 270 particles are arranged in a triangular close-packed lattice with periodic boundary conditions. In each calculation, the reduced volume $V^* = V/V_0$ ($V_0 = N\sigma^2\sqrt{3}/2$), reduced temperature $T^* = kT/\epsilon$, and step width c are fixed, and the reduced pressure $p^* = pV_0/N\epsilon$, the particle mean-square displacement $\langle R^2\rangle/\sigma^2$, and the coefficients A_n in the expansion[8] of the Helmholtz free energy are computed.

For the purpose of discussing the phase diagram, it is useful to divide the temperature into three regions: (1) $0.5 \lesssim T^* \leq \infty$, (2) $0.1 \lesssim T^* \lesssim 0.5$, and (3) $0 \leq T^* \lesssim 0.1$.

For temperatures $0.5 \lesssim T^* \leq \infty$, second-order perturbation theory accurately represents the phase boundaries. The Helmholtz free energy A and the pressure p are then given by

$$\frac{A(V^*, T^*)}{NkT} = \frac{A_0(V^*, T^*)}{NkT} + \frac{A_1(V^*)}{T^*} + \frac{A_2(V^*)}{T^{*2}} + \cdots,$$

$$\frac{p(V^*, T^*)V_0}{NkT} = \frac{p_0(V^*, T^*)V_0}{NkT} + \frac{p_1(V^*)}{T^*} + \frac{p_2(V^*)}{T^{*2}} + \cdots,$$

where p_0 is the hard-disk pressure and A_0 is the hard-disk free energy obtained by integrating p_0. The perturbation terms A_1 and A_2 have been computed in the hard-disk ($T^* = \infty$) limit for a series of c values and over a range of volumes. They have been fitted with smooth functions and differentiated to determine p_1 and p_2. Higher perturbation terms can be computed accurately only if A_2 is obtained at finite temperatures and is expanded to obtain A_3, A_4, etc.[8]

For the values of the step width investigated, namely $1.05 \leq c \leq 1.5$, A_1 varies monotonically from 3.0 (half the number of nearest neighbors) at $V^* = 1.0$ to zero at low density. Strong curvature is found in both A_1 and A_2 in the solid volume range $1 \leq V^* \leq 1.26$, and this leads to van der Waals loops and solid-solid phase transitions which terminate in critical points near $T^* = 1.0$. As c increases, the critical point of the solid-solid transition approaches the melting curve and eventually intersects it for $c \cong 1.30$. The curvature in $A_1(V^*)$ occurs at volumes where the number of neighboring particles separating from each other to distances $c\sigma$ is increasing rapidly. On the basis of a simple cell model, the volume corresponding to this point should be $V^* = c^2$, but the observed volumes are found to be much smaller than this. Thus $c = 1.2$ corresponds to a transition centered at $V^* \cong 1.13$ and $c = 1.3$ to a transition centered at $V^* \cong 1.2$. The surprising fact that the intersection of the solid-solid transition and the melting curve occurs at $c \cong 1.3$ rather than $c \cong 1.1$ as would be expected from the Lindemann melting law is no doubt connected with the long-wavelength modes characteristic of the two-dimensional solid. These modes lead to divergent mean-square displacements[9] and broad peaks in the pair distribution function. In three dimensions, where the collective fluctuations are much smaller, we expect a more realistic relationship between the step width and the volume at which the corresponding phase transition occurs.

Comparison of $A_1(V^*)$ values obtained from molecular dynamics with those computed from accurate pair distribution functions[10] shows good agreement. This indicates that number-dependence corrections are small, and that the 270-particle system is adequate for accurate calculations of phase boundaries.

In the temperature range $0.1 \lesssim T^* \lesssim 0.5$, second-order perturbation theory is no longer accurate, and direct finite-temperature calculations must be made to determine phase boundaries. The low-temperature solid-solid phase transition was clearly indicated by van der Waals loops in the isotherms. The melting curve was more difficult to determine, and the mean-square displacement $\langle R^2\rangle/\sigma^2$ proved to be useful in distinguishing the two phases. In the solid phase, $\langle R^2\rangle/\sigma^2$ will rapidly approach a constant value with time, whereas in the liquid phase $\langle R^2\rangle/\sigma^2$ will increase linearly with time as the particles diffuse. Extensive computer runs were required to map out the melting-curve extrema which occurred in this region.

For $T^* \lesssim 0.1$ molecular dynamics calculations are no longer useful because the system takes too long to reach thermodynamic equilibrium. Instead, phase boundaries in this region are computed by extrapolation of rigorous $T^* = 0$ results to higher temperature. Thus the melting curve near $T^* = 0$ represents a solid phase of disks of diameter $c\sigma$ in equilibrium with the corresponding fluid, and the low-temperature melting curve is then simply the high-temperature curve scaled down by a factor of c^2, or $p_m^* = 7.8\ T^*/c^2$. This

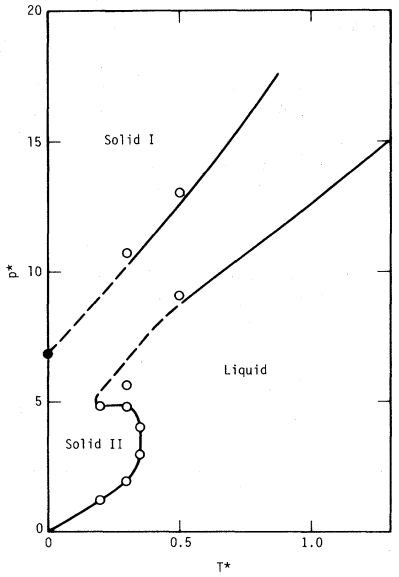

FIG. 2. The phase diagram for $c = 1.2$. The solid curves represent reliably determined phase boundaries obtained by various methods. Circles indicate finite-temperature molecular dynamics determinations of phase transitions. The dashed curves indicate uncertain phase boundaries.

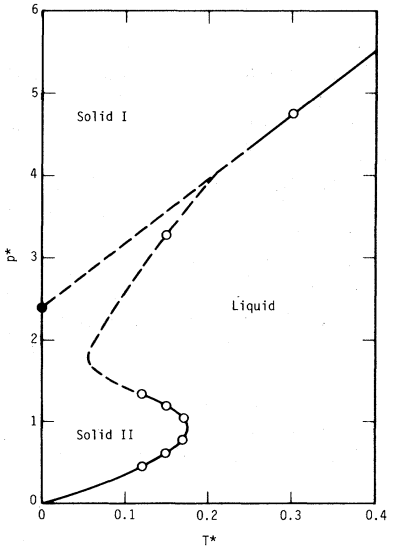

FIG. 3. The phase diagram for $c = 1.5$. The solid curves represent reliably determined phase boundaries determined by various methods. Circles indicate finite-temperature molecular dynamics determinations of phase transitions. The dashed curves indicate uncertain phase boundaries.

extrapolation agrees well with the observed melting curve at $T^* > 0.1$, as seen in Figs. 2 and 3. In addition, the solid-solid phase transition at $T^* = 0$ can be determined as the equilibrium between the high-density solid at $V^* = 1$ and the low-density solid at $V^* = c^2$, with the result that $p^* = 3/(c^2 - 1)$. This is in good agreement with the extrapolation of perturbation theory to lower temperatures, also as shown in Figs. 2 and 3.

The phase diagrams in Figs. 2 and 3 show isostructural solid-solid phase transitions and melting-curve extrema, thus confirming the suggestion that these phenomena are intimately linked and that they can be reproduced by the simple step potential. The most significant difference between the two diagrams is that for $c = 1.2$ the solid-solid transition ends in a critical point, while for $c = 1.5$ the transition intersects the melting curve in a triple point. This difference also corresponds to the main difference between the Ce and Cs phase diagrams. The analogy is not precise, however, because the solid-solid phase trajectories in the model do not point at or intersect the melting-curve minimum, as they do in Ce and Cs. This lack of qualitative agreement could be due to the simple, purely repulsive potential used.

The phase diagrams in Figs. 2 and 3 can be made somewhat more realistic by adding to the repulsive step potential an attractive term. If a square well of width 1.5σ is added to the $c = 1.2$ step potential, the effect on the phase diagram can be computed to first order in perturbation theory. Thus, if the depth of the square well is approximately three times the height of the step, then the phase boundaries are shifted downward so that the melting-temperature maximum falls below $p^* = 0$ and is eliminated. Although the solid-solid phase transition is only slightly affected by the perturbation, the result is much closer to the real cerium diagram. A similar transformation could introduce a solid-liquid-vapor triple point into the $c = 1.5$ phase diagram if a square well wider than 1.5σ were added to the potential.

In conclusion, it is clear that the step potential gives rise to phase diagrams qualitatively similar to those observed in Ce and Cs. Step-potential calculations in three dimensions will be presented in a future publication.

We thank Mary Ann Mansigh for the computer programming.

*Prepared for U. S. Energy Research and Development Administration under contract No. W-7405-Eng-

48.
[1]W. Klement, Jr., and A. Jayaraman, Prog. Solid State Chem. 3, 289 (1966); J. F. Cannon, J. Phys. Chem. Ref. Data 3, 781 (1974); D. A. Young, Lawrence Livermore Laboratory Report No. UCRL-51902, 1975 (unpublished).
[2]A. Jayaraman, Phys. Rev. 137, A179 (1965); E. A King, J. A. Lee, I. R. Harris, and T. F. Smith, Phys. Rev. B 1, 1380 (1970).
[3]G. C. Kennedy, A. Jayaraman, and R. C. Newton, Phys. Rev. 126, 1363 (1962); A. Jayaraman, R. C. Newton, and J. M. McDonough, Phys. Rev. 159, 527 (1967); D. B. McWhan and A. L. Stevens, Solid State Commun. 7, 301 (1969).
[4]R. Grover and B. J. Alder, J. Phys. Chem. Solids 35, 753 (1974); W. J. Carter, J. N. Fritz, S. P. Marsh, and R. G. McQueen, J. Phys. Chem. Solids 36, 741 (1975).
[5]A. W. Lawson and T. Y. Tang, Phys. Rev. 76, 301 (1949); R. Sternheimer, Phys. Rev. 78, 235 (1950).
[6]Y. Kuramoto and H. Furukawa, Prog. Theor. Phys. 47, 1069 (1972); D. A. Young, J. Chem. Phys. 58, 1647 (1973); T. Yoshida and S. Kamakura, Prog. Theor. Phys. 52, 822 (1974); C. E. Hecht and J. Lind, J. Chem. Phys. 64, 641 (1976); J. M. Kincaid, G. Stell, and E. Goldmark, J. Chem. Phys. 65, 2172 (1976); E. Brindeau, R. Levant, and J.-P. Hansen, "A Simple Model for Melting Curve Maxima," to be published.
[7]B. J. Alder, W. G. Hoover, and D. A. Young, J. Chem. Phys. 49, 3688 (1968).
[8]B. J. Alder, D. A. Young, and M. A. Mark, J. Chem. Phys. 56, 3013 (1972).
[9]D. A. Young and B. J. Alder, J. Chem. Phys. 60, 1254 (1974).
[10]D. G. Chae, F. H. Ree, and T. Ree, J. Chem. Phys. 50, 1581 (1969).

Cr^{5+} Coupling to Lateral Proton Configurations in KH_2AsO_4

J. Gaillard and P. Gloux*
Centre d'Etudes Nucléaires de Grenoble, Département Recherche Fondamentale 85X, F-38041 Grenoble Cedex, France
and
K. A. Müller
IBM Zurich Research Laboratory, CH-8803 Rüschlikon, Switzerland
(Received 28 March 1977)

Electron-nuclear double-resonance (ENDOR) spectra at 1.5 K of $Cr^{5+}(3d^1)$ on tetrahedral As^{5+} sites in KH_2AsO_4 show lateral Slater protonic configurations. The $d_{x^2-y^2}$ function couples with the two near protons. The reorientation of this unit in the four possible lateral configurations occurs in the paraelectric phase. The observed reorientation times are discussed.

The coupling of lattice defects to collective modes is a subject of considerable interest. Recently, linear interactions of slowly relaxing defects with soft modes have been considered as a possible cause for slow central-peak dynamics near structural phase transitions by Halperin and Varma.[1] EPR investigations of Cr^{5+} in KH_2AsO_4 have shown the existence of slow local reorientation times shifting proportional to the Curie temperature T_C.[2] The two slow relaxation times τ and τ_ψ and the symmetry of the x^2-y^2 ground-state wave function indicated a Halperin-Varma-type center,[3] i.e., a linear interaction with the soft protonic mode. Hereafter, and electron-nuclear double-resonance (ENDOR) study is reported which aimed at elucidating this interaction with the protons. Its main result is that the $d_{x^2-y^2}$ function couples simultaneously with the two near protons in lateral Slater configurations at low temperatures, which proves the existence of a reorientation among these four configurations—a unique situation not reported before in the high-temperature phase of this class of hydrogen-bonded ferroelectrics.

The Cr^{5+}-doped KH_2AsO_4 samples used in this study were identical with the ones used previously.[2] The proton ENDOR spectra were run at 1.5 K in an X-band spectrometer as described elsewhere.[4] A typical spectrum for $\vec{H}\parallel\vec{c}$ upon saturation of the center of the single paramagnetic resonance line is shown in Fig. 1. It is seen that, symmetrically to the line for very distant protons, there are two pairs denoted by $\{3^+,3^-\}$ and $\{4^+,4^-\}$ which could be identified with two far protons of the CrO_4^{3-} tetrahedron. The lines $\{2^+,2^-\}$ and 1^- result from two near protons of the tetrahedron. The 1^+ transition occurs at too low a frequency to be observed. The above assignments were obtained from the angular variations recorded. The sign + or − indicates the electronic